Optimization Methods for Wireless Power Transfer

Lavinia Bobaru, Mihai Iordache, Marilena Stanculescu, Dragos Niculae, and Sorin Deleanu

Abstract This chapter provides an investigation of the wireless power transfer domain. It follows the description of the analysis and identification of the system's parameters, which consist of two magnetically connected coils utilized in constructing the wireless power transfer system. A section of this chapter focuses on the optimization aspects of the wireless energy transfer. The optimization considers a function of several parameters of the system such as the structure, the number of turns, the WPTS's working frequency.

Keywords Wireless power transfer · Optimization · Magnetic couplings · Parameter identification

Nomenclature

A. Acronyms

WPT	Wireless Power Transfer
WEP	Wireless Energy Transfer
SCORs	Strongly Coupled Resonances

L. Bobaru · M. Iordache · M. Stanculescu (✉) · D. Niculae
Department of Electrical Engineering, University Politehnica Bucharest, Bucharest, Romania
e-mail: marilena.stanculescu@upb.ro

L. Bobaru
e-mail: lavinia.bobaru@upb.ro

M. Iordache
e-mail: mihai.iordache@upb.ro

D. Niculae
e-mail: dragos.niculae@upb.ro

S. Deleanu
Northern Alberta Institute of Technology, Edmonton, Canada
e-mail: sorind@nait.ca

N. Mahdavi Tabatabaei and N. Bizon (eds.), *Numerical Methods for Energy Applications*, Power Systems,
https://doi.org/10.1007/978-3-030-62191-9_20

MIT	Massachusetts Institute of Technology
MM	Fmagnetomotive force
EMF	Electromotive force
AC	Alternating current
ss	series-series configuration
pp	parallel-parallel configuration
sp	series-parallel configuration
ps	parallel-series configuration
APL	active power transmitted to the load

B. Symbols/Parameters

$u_{m\Gamma}$	magnetomotive force
i_{S_Γ}	conduction electric current strength
Ψ_{S_Γ}	electric flux
Θ_{S_Γ}	turn
H	magnetic field strength (intensity)
J	current density
B	magnetic flux density (induction)
D	electric displacement
Φ_{S_Γ}	magnetic flux
E	electric field strength
$\overline{w}$	local speed vector of the medium
u_{Γ}	EMF
u_t	EMF induced by transformation
u_m	EMF induced by movement
R	resistance
L	inductivity
C	capacity
M	mutual inductivity
R	the matrix of resistive coefficients
L	the matrix of inductive coefficients
C	the matrix of capacitive coefficients
r	initial radius of the turn
p	pitch (distance between two consecutive turns)
h	the distance between the two coils along Oz axis
N_1, N_2	the number of turns for coil 1, respectively, for coil 2
f	frequency
$H(f)$	transfer function
g_j	objective function
P	power
η	efficiency
(Γ)	closed curve
(S_Γ)	open surface
(Σ)	closed surface

$\overline{dA}$ area element
$\overline{dl}$ line element

1 Introduction to Wireless Power Transfer

Wireless Power Transfer (WPT) or Wireless Energy Transfer (WEP) represents a new technology, suitable to bring electricity to places where the utilization of system interconnection via cables is either difficult, impractical or even impossible. Although the WPT is ineffective for large distances [1, 2] due to the electromagnetic field weakness [3], there is the possibility to achieve a more efficient power transfer if the emitting coil (emitter) and the receiving coil (receiver) are at resonance [5, 6]. Both the electromagnetism and the electric circuit theory recognize the condition of "resonance" for the best efficiency possible regarding the power transfer.

Despite a total power loss counting for 30% of the transferred power, WPT has numerous applications [7–9] such as:

- *Medical implants*. Technological progress in the field of biomedical allowed the creation of biomedical implants such as pacemakers, cochlear implants, subcutaneous drug supply implants
- *Chargers* used for smartphones, electric and hybrid vehicles, unmanned aerial vehicles.
- *Appliances* such as ironing, vacuum cleaner, TV.

Currently, there are three types of WPTs: *radiant transfer*, *inductive transfer*, and *resonant coupling transfer*. In the case of radiant transfer, most of the generated power is lost in surrounding space. In contrast, the received power comes in small amounts (i.e., in order of mW), making the radiant transfer suitable for the transmission of information. Regarding the inductive coupling [5], the power transfer can be very efficient, although the distance emitter-receiver is only in terms of a few centimeters. The application of the resonant coupling method allows the transfer of significant power over relatively long distances (few meters). The experimental studies carried out at MIT led to a potential breakthrough in WPT. The researchers proposed a new scheme based on the concept named Strongly Coupled Resonances (SCORs) [6, 9]. The fundamental principle of this type of transmission is based on the idea that resonant objects exchange energy, whereas the non-resonant ones do not realize such an energy transfer [7, 8]. The WPT transformation from concept into large scale applications occurred relative recently, although one can track the first research works on the subject back in the 1880s [8]. Energy transmission without galvanic contacts did not become an established technique yet, capable of operating with clear solutions, design methods, and regulated practices. For example, only a few years ago (2012), WPT had a real narrow niche, its applications addressing the cell phones and digital tablets, only. However, later, in 2015, the WPT market considerably expanded, its value reaching 1 billion dollars. There are predictions in

place [10], suggesting that the WPT market would reach a value of 5 billion dollars by 2020. A WPT market dominated by ordinary small customers is in sight for the future, no matter the real big business desire for a significant WPT expansion in the industry in general, and the automotive sector.

The chapter starts by analyzing the current literature and by presenting the different wireless power transfer methods together with their corresponding applications, which varies from domains such as the medical one up to the military one. It follows the description of the analysis and identification of the system's parameters, which consist of two magnetically connected coils utilized in constructing the wireless power transfer system.

A section of this chapter focuses on the optimization aspects of the wireless energy transfer. The optimization requires the consideration of several aspects. It is presented the WPTS's optimization by using the transfer function method. The optimization method for the system consisting of the two magnetically coupled coils and used in WPTS considers a function depending on several parameters of the system, such as the structure, the number of turns, the WPTS's working frequency.

Electromagnetic energy wireless transfer is a developing, emerging technology, resulted from the significant progress in the power electronics domain. The possible applications of this technology present an enormous potential, which may influence the way we use the current applications.

Despite the fact there are vital signs of progress in this domain, we are still far from reaching this objective, due to the significant design challenges. The small efficiency and the limited range of transfer are two of the most crucial aspect which must be improved.

The chapter ends with conclusions and many references in the field of wireless power transfer.

2 Theoretical Considerations

The WPT systems operate according to two fundamental principles:

- The magnetic circuit law (Ampere's Law)
- The electromagnetic induction law (Faraday-Lenz Law).

The magnetic circuit law(Ampère's Law), according to [11], has the initial definition mathematically summarized in the differential form (3.1). The magnetic circuit law consists of the following statement:

The magnetomotive force (MMF), $u_{m\Gamma}$, along any closed curve (Γ) is equal to the sum between the *conduction electric current strength* i_{S_Γ} through an open surface (S_Γ) arbitrary chosen, bordered by the closed curve (Γ) and the *time derivative of the electric flux* Ψ_{S_Γ} over the same surface: (S_Γ)

$$u_{m_\Gamma} = i_{S_\Gamma} + \frac{d\Psi_{S_\Gamma}}{dt} \tag{1}$$

The term i_{S_Γ} is also called turn, and denoted by Θ_{S_Γ}.

By rewriting relation (1), one obtains the integral form of Ampere's law (2):

$$\int\limits_{(\Gamma)} \overline{H} \cdot \overline{dl} = \int\limits_{(S_\Gamma)} \overline{J} \cdot \overline{dA} + \frac{d}{dt} \int\limits_{(S_\Gamma)} \overline{D} \cdot \overline{dA} \tag{2}$$

The integral form is valid only in the context of the application of the corkscrew rule between the reference direction, the oriented line element $\overline{dl}$, and the oriented area element $\overline{dA}$ This observation applies concerning the electromagnetic induction law as well. For domains with continuity, one can modify the relation (2) according to the properties of the operators into (3).

$$curl\overline{H} = \overline{J} + \frac{\partial \overline{D}}{\partial t} + \overline{w} \cdot \rho_v + curl\left(\overline{D} \times \overline{w}\right) \tag{3}$$

The last form is the magnetic circuit law expressed in the local (punctual) form:

For stationary media $\overline{w} = 0$ the local form becomes:

$$curl\overline{H} = \overline{J} + \frac{\partial \overline{D}}{\partial t} \tag{4}$$

According to (4), one can affirm that the closed lines of the magnetic field border the entities responsible for its generation:

- The wires transited by conduction currents.
- The lines of the time variable electric field that generates them.

The electromagnetic induction law (Faraday's law) has the following statement [11]:

The electromotive force (EMF) u_Γ along a closed curve (Γ) is equal to the negative of the time derivative of the magnetic flux Φ_{S_Γ} across any surface (S_Γ) bordered by the closed curve (Γ):

$$u_\Gamma = -\frac{d\Phi_{S_\Gamma}}{dt} \tag{5}$$

Note: The form presented in (5) includes the adjustment represented by the "negative" sign introduced by Lenz.

Considering the definition relations of EMF, respectively of the magnetic flux, one can extrapolate (8) into the integral form of the Faraday-Lenz law (6):

$$\int\limits_{(\Gamma)} \overline{E} \cdot \overline{dl} = -\frac{d}{dt} \int\limits_{(S_\Gamma)} \overline{B} \cdot \overline{dA}. \tag{6}$$

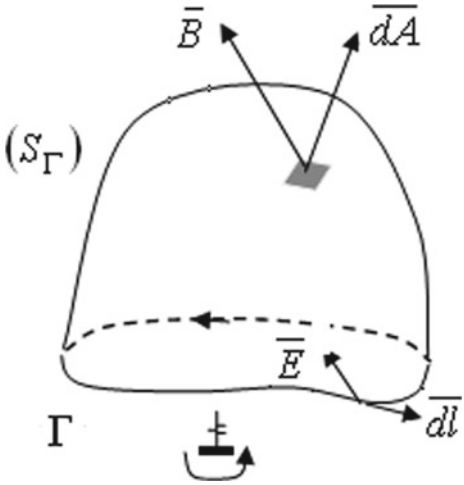

Fig. 1 The Electromagnetic induction law

The integral for of the electromagnetic induction law is valid only when fulfilling the condition: the reference direction of the closed curve (Γ) (i.e., the reference direction of the oriented line element $\overline{dl}$) and the direction of the normal to the surface (S_Γ) (i.e., the oriented area element $\overline{dA}$)) comply with the right corkscrew rule (see Fig. 1).

For mobile media, the integration domains follow the bodies in their movement, and the time derivative of the magnetic flux becomes a substantial derivative and it is computed using the following relation:

$$\frac{d}{dt}\int\limits_{(S_\Gamma)} \overline{B}\cdot\overline{dA} = \int\limits_{(S_\Gamma)} \left[\frac{\partial \overline{B}}{\partial t} + \overline{w}\cdot div\,\overline{B} + curl\left(\overline{B}\times\overline{w}\right)\right]\cdot\overline{dA}, \tag{7}$$

In (7), $\overline{w}$ is the local speed vector of the medium.

Using Stoke relation, results:

$$\int\limits_{(\Gamma)} \overline{E}\cdot\overline{dl} = \int\limits_{(S_\Gamma)} \left(curl\,\overline{E}\right)\cdot\overline{dA} \tag{8}$$

Considering the local form of the magnetic flux law, one obtains a new integral form of the Faraday's law of electromagnetic induction:

$$u_\Gamma = \int\limits_{(\Gamma)} \overline{E}\cdot\overline{dl} = -\int\limits_{(S_\Gamma)} \frac{\partial \overline{B}}{\partial t}\cdot\overline{dA} - \int\limits_{(\Gamma)} \left(\overline{B}\times\overline{w}\right)\cdot\overline{dl} \tag{9}$$

The physical significance of the law: the time-variable magnetic field produces (induces) an electric field through the electromagnetic induction. Therefore, the electromagnetic induction is a physical phenomenon, unlike electric the flux density $\overline{D}$ and magnetic induction $\overline{B}$, which are physical quantities.

Furthermore, the decomposition of the EMF in two components:

$$u_\Gamma = u_t + u_m \tag{10}$$

With

$$u_t = -\int\limits_{(S_\Gamma)} \frac{\partial \overline{B}}{\partial t} \cdot \overline{dA} = \int\limits_{(S_\Gamma)} \left(-\frac{\partial \overline{B}}{\partial t}\right) \cdot \overline{dA} \tag{11}$$

called electromotive force (EMF) induced by transformation and, respectively,

$$u_m = -\int\limits_{(\Gamma)} \left(\overline{B} \times \overline{w}\right) \cdot \overline{dl} = \int\limits_{(\Gamma)} \left(\overline{w} \times \overline{B}\right) \cdot \overline{dl} \tag{12}$$

called EMF induced by movement.

The two components reveal the two forms of electromagnetic induction:

- time variation of the magnetic induction $\overline{B}$, with no movement u_t
- at least a portion of the closed curve (Γ) is mobile in the space containing magnetic field u_m.

The simultaneous application of both laws, the magnetic circuit law, and the electromagnetic induction one, detailed above, provide the proper frame for WPT development. The wireless transfer of the electromagnetic power requires the presence of, at least, two magnetically coupled coils, a fact which labels WPTs as inductive power transfer systems.

A simple explanation of the WPT operation is:

- An AC flowing through a coil (called primary coil, source or transmitter) produces an AC magnetic field, having the same frequency of the current.
- The AC magnetic field due to the primary coil sweeps the closed surface bordered by another coil (called secondary coil, resonator device, or receiver) placed about the primary one and induces an EMF across the receiver transferred inductively, [12–18] (see Fig. 2).

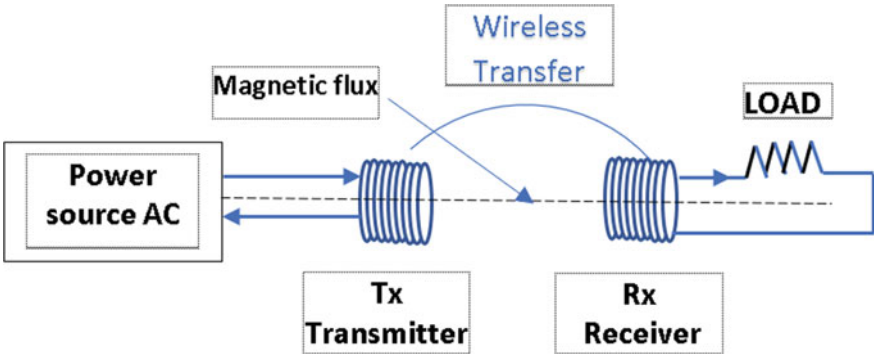

Fig. 2 Schematic view of a WPTS

3 Parameters Identification for the Wireless Power Transfer

Several literature resources identified the pancake type of coils as suitable for applications regarding battery charging solutions [19–24]. Assuming that for every structure emitter-receiver (two coils magnetically coupled), the number of turns, geometrical dimensions, and the fabrication materials remain the same (the frequency is the variable of interest). Following theoretical and experimental tests, one can conclude that the structure with the value of the mutual inductivity represents the optimal coupling solution [19–29]. A method exemplifying the optimization process applied to the configuration with two magnetically coupled coils utilized the ANSYS Q3D Extractor software [30–32]. According to this method, there is a set of matrices $\boldsymbol{R}$, $\boldsymbol{L}$, $\boldsymbol{C}$, and $\boldsymbol{G}$, representing the resistive, inductive, capacitive, respectively coupling coefficient elements. The representation of the last matrix, $\boldsymbol{G}$, becomes a simple number. The assessment of several possible solutions of coupled coils utilized in WPT, concerning configurations, structures, and frequencies guides the designer, finally, to the optimum one. The frequency values of interest in these simulations are 50, 5000, and 10,000 kHz, whereas the four analyzed configurations with their parameters appear in Figs. 3, 4, 5, 6.

3.1 The Assessment of Two Parallel-Bases Helicoidally Pancake-Type Coils

The two coils (see Fig. 3) have the following geometrical parameters:

- Initial radius of the turn $r = 10\ mm$
- Pitch (distance between two consecutive turns) on OY axis $p = 1.3\ mm$
- Section of the conductors $s = 1.2\ mm \times 0.8\ mm = 0.96mm^2$

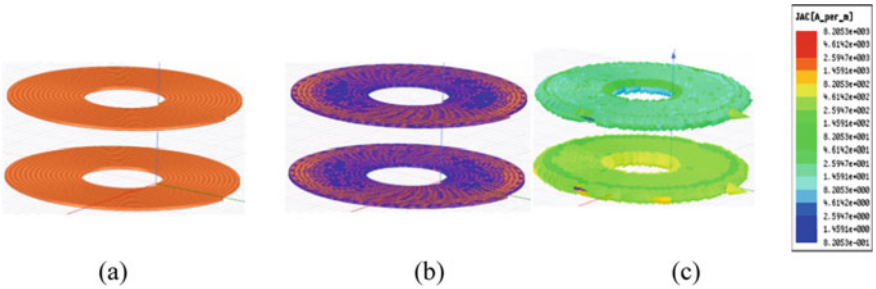

Fig. 3 **a** The structure of the two helicoidally coils with parallel bases; **b** The distribution of the discretization points; **c** Current sheet distribution

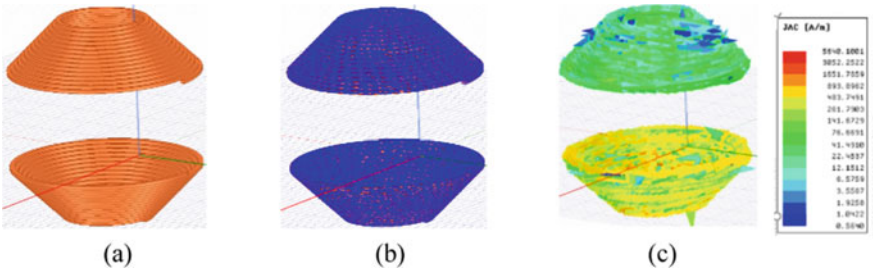

Fig. 4 **a** The structure of the two coils truncated cone-like with parallel bases **b** Distribution of discretization points; **c** Distribution of current sheet

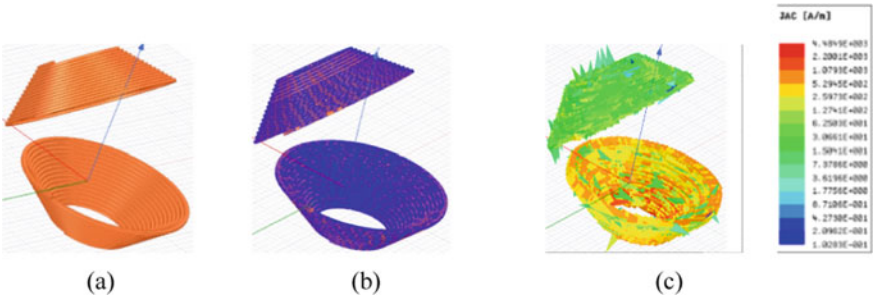

Fig. 5 **a** The structure of the two coils truncated cone-like with non-parallel bases, one rotated 450; **b** Distribution of discretization points; **c** Distribution of current sheet

- Distance between the two coils along Oz axis $h = 20\ mm$
- Number of turns $N_1 = N_2 = 15$.

The identification of electric parameters (i.e., ohmic resistances, parasitic capacitances, self-inductivities, as well as the coupling coefficient) filled in for Table 1.

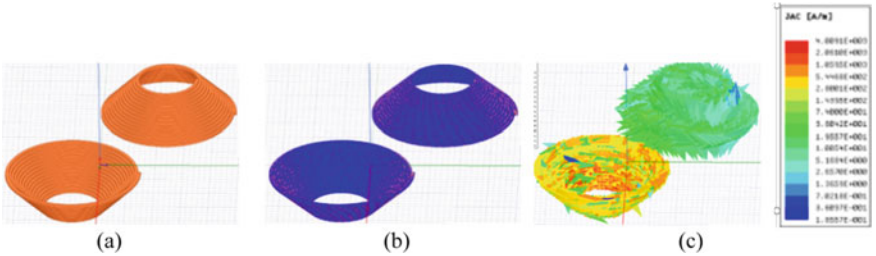

Fig. 6 **a** The structure of the two truncate cone-like coils, with parallel bases, z = 20 mm and y = 15 mm; **b** Distribution of the discretization points; **c** Distribution pf current sheet

Table 1 The electric parameters for two helicoidally pancake coils with parallel basis

Frequency f [kHz]	50	5000	10,000
Resistance matrix [ohm]	$\begin{pmatrix} 0.72029 & 0.26477 \\ 0.26477 & 0.72313 \end{pmatrix}$	$\begin{pmatrix} 0.20907 & 0.02964 \\ 0.02964 & 0.20839 \end{pmatrix}$	$\begin{pmatrix} 2.9425 & 0.41043 \\ 0.41043 & 3.0142 \end{pmatrix}$
Inductivity matrix [μH]	$\begin{pmatrix} 8.0489 & 1.5812 \\ 1.5812 & 8.0487 \end{pmatrix}$	$\begin{pmatrix} 6.8438 & 0.26477 \\ 0.63748 & 6.7874 \end{pmatrix}$	$\begin{pmatrix} 6.6993 & 0.62623 \\ 0.62623 & 6.6878 \end{pmatrix}$
Capacity matrix [pF]	$\begin{pmatrix} 3.1308 & -1.7213 \\ -1.7213 & 3.1325 \end{pmatrix}$	$\begin{pmatrix} 3.1308 & -1.7213 \\ -1.7213 & 3.1325 \end{pmatrix}$	$\begin{pmatrix} 3.1308 & -1.7213 \\ 0.2648 & 3.1325 \end{pmatrix}$
Coupling coefficient [μH]	0.19646	0.19646	0.19742

3.2 *The Assessment of Two Truncated Cone-Like Coils, with Parallel Bases, Configuration a*

The two coils (see Fig. 4) have the following geometrical parameters:

- Turn's initial radius $r = 10$ mm
- Pitch on OY axis $p = 0.9$ mm
- Section of the conductors $s = 1.2 \times 0.8 = 0.96$ mm^2
- Distance between the two coils along Oz axis $h = 20$ mm
- Number of turns $N_1 = N_2 = 15$.

The identification of electric parameters (i.e., ohmic resistances, parasitic capacitances, self-inductivities, as well as the coupling coefficient) are filled in for Table 2.

Table 2 The electric parameters for two truncated cone-like coils with parallel basis, configuration A

Frequency f [kHz]	50	5000	10,000
Resistance matrix [ohm]	$\begin{pmatrix} 0.72029 & 0.26477 \\ 0.26477 & 0.72313 \end{pmatrix}$	$\begin{pmatrix} 1.2159 & 0.12714 \\ 0.12714 & 1.4602 \end{pmatrix}$	$\begin{pmatrix} 2.0539 & 0.211247 \\ 0.21124 & 1.7596 \end{pmatrix}$
Inductivity matrix [μH]	$\begin{pmatrix} 6.7639 & 0.63251 \\ 0.63251 & 6.7609 \end{pmatrix}$	$\begin{pmatrix} 6.8438 & 0.26477 \\ 0.63748 & 6.7874 \end{pmatrix}$	$\begin{pmatrix} 6.7947 & 0.63513 \\ 0.63513 & 6.8295 \end{pmatrix}$
Capacity matrix [pF]	$\begin{pmatrix} 3.1309 & -1.7213 \\ -1.7213 & 3.1325 \end{pmatrix}$	$\begin{pmatrix} 2.376 & -1.0406 \\ -1.0406 & 2.3759 \end{pmatrix}$	$\begin{pmatrix} 3.1308 & -1.7213 \\ -1.7213 & 3.1325 \end{pmatrix}$
Coupling coefficient [μH]	0.093534	0.093533	0.093236

3.3 The Assessment of Two Truncated Cone-Like Coils, with Non-Parallel Bases with One Coil Rotated 45^0.

The two coils (see Fig. 5) have the following geometrical parameters:

- Turn's initial radius $r = 10$ mm
- Pitch on OY axis $p = 0.9$ mm
- Section of the conductors $s = 1.2 \times 0.8 = 0.96$ mm^2
- Distance between the two coils along Oz axis $h = 20$ mm
- Number of turns $N_1 = N_2 = 15$.

The identification of electric parameters (i.e. ohmic resistances, parasitic capacitances, self-inductivities as well as the coupling coefficient) filled in for Table 3

Table 3 The electric parameters for two truncated cone-like coils with non-parallel bases, one coil rotated 45^0

Frequency f [kHz]	50	5000	10,000
Resistance matrix [ohm]	$\begin{pmatrix} 0.20907 & 0.029635 \\ 0.029636 & 0.20839 \end{pmatrix}$	$\begin{pmatrix} 0.20907 & 0.029635 \\ 0.029636 & 0.20839 \end{pmatrix}$	$\begin{pmatrix} 2.9425 & 0.41043 \\ 0.41043 & 3.0142 \end{pmatrix}$
Inductivity matrix [μH]	$\begin{pmatrix} 6.7639 & 0.63251 \\ 0.63251 & 6.7609 \end{pmatrix}$	$\begin{pmatrix} 6.8438 & 0.26477 \\ 0.63748 & 6.7874 \end{pmatrix}$	$\begin{pmatrix} 6.6993 & 0.62623 \\ 0.62623 & 6.6878 \end{pmatrix}$
Capacity matrix [pF]	$\begin{pmatrix} 3.1309 & -1.7213 \\ -1.7213 & 3.1325 \end{pmatrix}$	$\begin{pmatrix} 2.376 & -1.0406 \\ -1.0406 & 2.3759 \end{pmatrix}$	$\begin{pmatrix} 2.376 & -1.0406 \\ -1.0406 & 2.3759 \end{pmatrix}$
Coupling coefficient [μH]	0.092983	0.092983	0.093557

Table 4 The electric parameters of 2 truncate cone-like coils, with parallel bases, configuration B

Frequency f [kHz]	50	5000	10,000
Resistance matrix [ohm]	$\begin{pmatrix} 0.2042 & 0.0056 \\ 0.0056 & 0.2031 \end{pmatrix}$	$\begin{pmatrix} 2.0238 & 0.05731 \\ 0.057309 & 2.0168 \end{pmatrix}$	$\begin{pmatrix} 2.8266 & 0.0802 \\ 0.0802 & 2.8088 \end{pmatrix}$
Inductivity matrix [μH]	$\begin{pmatrix} 6.7052 & 0.12503 \\ 0.1250 & 6.7051 \end{pmatrix}$	$\begin{pmatrix} 6.6964 & 0.6213 \\ 0.1244 & 6.6968 \end{pmatrix}$	$\begin{pmatrix} 6.7280 & 0.6262 \\ 0.1260 & 6.7324 \end{pmatrix}$
Capacity matrix [pF]	$\begin{pmatrix} 2.1893 & -0.7505 \\ -0.7505 & 2.1895 \end{pmatrix}$	$\begin{pmatrix} 2.1893 & -0.7505 \\ -0.7504 & 2.1895 \end{pmatrix}$	$\begin{pmatrix} 2.1893 & -0.7505 \\ -0.7505 & 2.1895 \end{pmatrix}$
Coupling coefficient [μH]	0.01865	0.01863	0.01871

3.4 The Assessment of Two Truncated Cone-Like Coils, with Parallel Bases, Configuration B

The two coils (see Fig. 6) have the following geometrical parameters:

- Turn's initial radius $r = 10$ mm
- Pitch on OY axis $p = 0.9$ mm
- Section of the conductors $s = 1.2 \times 0.8 = 0.96$ mm^2
- Distance between the two coils along Oz axis $h = 20$ mm
- Number of turns $N_1 = N_2 = 15$.

From the four configurations of the two magnetically coupled coils under investigation, one can remark the highest mutual inductivity of $M = \mu H$ (see Table 1), a fact which indicates the configuration from 20.2.1 as the optimum. MATLAB software package, as a universal standard for scientific applications, proved very attractive for the elaboration of efficient procedures aiming for the numerical calculation of the mutual inductance corresponding to the two magnetically coupled coils [33–41].

4 The Optimization of Parameters

The most straightforward configuration of a WPT system consists of two magnetically coupled coils (transmitter and receiver). This configuration can be *series – series (ss), parallel – parallel (pp), series–parallel (sp) and parallel – series (ps).* The transmitter releases a non-radiant magnetic field with an oscillation frequency in the full range of *30 kHz – 40 MHz*. In this way, between the receiver and transmitter (*assumed in magnetic resonance*), it is ensured an efficient power transfer. A generally accepted statement from the literature [1–10], claims that the magnetic interaction between

the transmitter (source) and the receiver must be *strong enough*, making it possible to neglect the other magnetic interactions with non-resonant objects.

The result is an efficient channel for WPT. Available studies [4, 6] show that WPT doesn't change noticeably, in the presence of people or various objects placed between the two coils or in their close neighborhood. This statement is also valid for the case when these objects completely cover the direct line between the transmitter and the receiver. Some materials, such as aluminum, can produce changes in the resonance of their resonance frequency, but the correction of this issue is relatively easy by using a reaction circuit. WPT offers the possibility of connecting the electronic devices without wires, a fact that determines a reduction in the dimensions of the equipment, accompanied by a cost reduction. Both the amount of transferred between two coils and the WPT efficiency strongly depend on their parameters.

The *maximum transmitted active power* or the *maximum transmission efficiency* counts as criteria meant to determine the optimum values for the magnetically coupled coils. The next section contains a presentation of two optimization methods, based on the *transfer functions*, respectively, the *output square error.* The MATLAB functions (from MATLAB toolbox) that can be used are the minimization functions "*fminimax*", "*fminunc*" [38].

4.1 Transfer Function and Output Square Error Method Based on "fminunc" Function

The system under study consist of a system composed of two series-series resonators (magnetically coupled, no wires) used in inductive WPT as in Fig. 7.

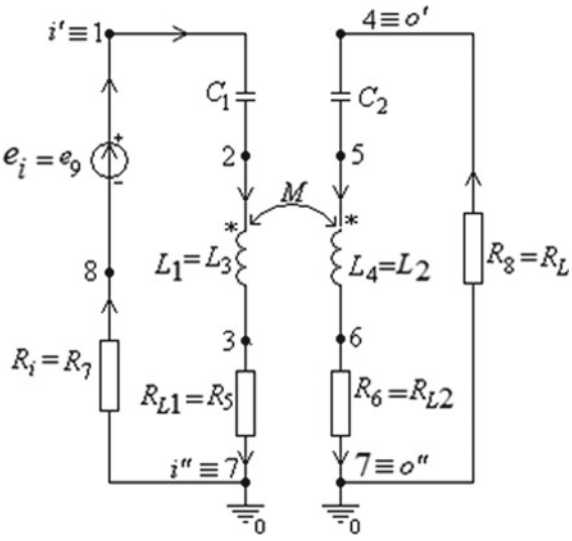

Fig. 7 Two series-series resonators magnetically coupled, powered by an AC voltage source

One can look to the circuit as being a two-port system operating in the frequency domain. There are several possibilities to optimize the WPT for this system, utilizing one of the functions: *useful active power transmitted to the load* (APL), *power transmission efficiency*, *signal transmission efficiency*, or *any other transfer function* [39, 40]. From the equivalent scheme of an analog two-port system in the AC regime, one can achieve any complex transfer function *H(jw)*, expressed either in an entirely *symbolic form*, *partially symbolic* or *numeric*. The measurements are targeting the absolute value of the phase angle imposed by the system energization from a voltage source with variable frequency capabilities. *H(f)* is the transfer function (or the output quantity) in an entirely symbolic form using the software developed and explained in [36, 37]. The system's parameters chosen for optimization or identification are $x_1, x_2, \ldots, x_p$ (p - the number of unknowns). The remained $(n-p)$ parameters come as nominal values taken from the catalog. Whereas considering k frequency samples at which the circuit function is available through measurements or simulations (the output function or any other circuit performance quantity), one can formulate the following objective function as in (13) and (14):

$$g_j(x_1, x_2, \ldots, x_p, f_j) = \left(\left|\underline{H}(f_j)\right| - \left|\underline{H}(f_j, x_1, x_2, \ldots x_p)\right|\right)^2,\ j = \overline{1,k} \tag{13}$$

$$f(x_1, x_2, \ldots, x_p) = \sum_{j=1}^{k} \left(\left|\underline{H}(f_j)\right| - \left|\underline{H}(f_j, x_1, x_2, \ldots, x_p)\right|\right)^2 \tag{14}$$

For a scalar objective function, k can be 1. When the objective function is the useful power P_2 or the efficiency $\eta = (P_2/P_1)100$ $\eta_{21} = \frac{P_2}{P_1} \cdot 100$, then the objective function has one of the following structures (15):

$$f(x_1, x_2, \ldots, x_p) = \sum_{j=1}^{k} \left(P_2(x_1, x_2, \ldots, x_p, f_j) - P_2(f_j)\right)^2 \tag{15a}$$

$$f(x_1, x_2, \ldots, x_p) = \sum_{j=1}^{k} \left(\eta_{21}(x_1, x_2, \ldots, x_p, f_j) - \eta_{21}(f_j)\right)^2, k \le 3 \tag{15b}$$

$$f(x_1, x_2, \ldots, x_p) = \sum_{j=1}^{k} \left(P_2(x_1, x_2, \ldots, x_p, f_j) - P_2(f_j)\right) \tag{15c}$$

$$f(x_1, x_2, ..., x_p) = \sum_{j=1}^{k} \left(\eta_{21}(x_1, x_2, ..., x_p, f_j) - \eta_{21}(f_j)\right), k \leq 3 \quad (15d)$$

In conditions of constant (fixed) frequency, the optimization functions become (16)

$$f(x_1, x_2, ..., x_p) = \left(P_2(x_1, x_2, ..., x_p, f) - P_2(f)\right)^2 \quad (16a)$$

$$f(x_1, x_2, ..., x_p) = \left(\eta_{21}(x_1, x_2, ..., x_p, f) - \eta_{21}(f)\right)^2 \quad (16b)$$

$$f(x_1, x_2, ..., x_p) = \left(P_2(x_1, x_2, ..., x_p, f) - P_2(f)\right) \quad (16c)$$

$$f(x_1, x_2, ..., x_p) = \left(\eta_{21}(x_1, x_2, ..., x_p, f) - \eta_{21}(f)\right) \quad (16d)$$

Usually, the quantity *H(f)* is a rational function which depends on frequency. The coefficients of the polynomials form the numerator and denominator of the transfer function (output quantity) are involved, consisting of multiplicators of parameters. The functions *fminimax* from MATLAB toolbox [38], solve a minimax problem under certain constraints.

5 Case Study: Optimization of Magnetically Coupled Coils

5.1 *Optimization of Useful Active Power $P_2 = P_{RL}$ Depending on the Parameters L_1, L_2, and M*

One can perform the analysis of the circuit from Fig. 7 in the frequency domain. The series-series connection exemplified by the circuit from Fig. 7 is the most efficient with respect to the WPT [6, 7]. The geometric dimensions of the two coils are: $r = 150$ mm, $p = 3$ mm, $w = 2$ mm (the conductor's diameter), $g = 150\ mm$ (the distance between the coils), $N_1 = N_2 = 5$ (the turn's number). Using ANSOFT EXTRACTOR Q3D (ANSYS) [38], the numerical values of the two coils magnetically coupled (Fig. 7) are:

$$
\begin{aligned}
&PLss_f = 61342RLf^0C2^2M^2C2^2Ei^2 \Big/ \Big[F_1 f^8 + (F_2 + F_3) f^6 + F_4 f^4 + F_5 f^2 + F_6\Big] \\
&F_1 = (1 + (-0.48 * 10^7 C1^2 L1 C2^2 L2 M^2 + 0.24 C2^2 M^4 C1^2 + 0.24 C1^2 L1^2 C2^2 L2^2) \\
&F_2 = 122684(RLRL1C1^2M^2 + C1^2RiC2^2RL2M^2 - C1^2L1^2C2^2L2 + ... \\
&C1^2L1^2C2^2RL2RL + C2^2L2M^2C1 + C1^2RiC2^2L2RL1 + C1^2RiC2^2M^2 ... \\
&\quad + RL1C1^2C2^2RL2M^2 - C1L1C2^2L2^2 + C1^2L1C2M^2) \\
&F_3 = 61342(RL1^2C1^2C2^2L2^2 + C1RiC2^2L2^2 + C1^2L1^2C2^2 + C1^2L1^2C2^2RL2^2) \\
&F_4 = 3111(RL2C1^2RiC2^2RL1 - C2^2M2C1 + RLRL1^2C1^2C2^2RL2 - RL2C1L1C2^2 \\
&... + RLC1^2RL2 - C1^2RiC2L2 + RL1C1^2C2^2RL2^2Ri - C1^2RL1^2C2L2 - C2^2RL2^2C1L1) \\
&F_5 = [79(-C1L1 - C2L2 + C1^2RiRL1 + C2RL2RL)] \\
&F_6 = 6222(C1L1C2L2 + RLC1^2RiRL1RL2 - C1^2RiRL1C2L2 - C2^2RL2RLC1L1) ... \\
&\quad + 1555(C2^2L2^2 + RL2RL1^2C1^2C2^2 + C1^2Ri2C2^2RL2^2 + RL1^2C1^2C2^2RL2^2 ... \\
&\quad + C1^2L1^2 + RL2C1^2Ri2C2^2) + 39(C2^2RL2 + C2^2RL2^2 + C1^2Ri2 + RL1^2C1^2)
\end{aligned}
\tag{17}
$$

In conditions of unknown L_1, L_2, M, and frequency f, the expression of the load transferred active power is (18)

$$
\begin{aligned}
&PLss\_L1L2M\_PRL := 0.23 \cdot 10^{-33} f^6 M^2 \Big/ \Big[1 + (T_1 + T_4) \cdot f^8 + T_2 f^6 + T_3 f^4\Big] \\
&T_1 = 0.24 \cdot 10^7 \Big(-0.75 \cdot 10^{-43} L1\, L2 M^2 + 0.37 \cdot 10^{-43} M^4 + 0.37 \cdot 10^{-43} L1^2 L2^2\Big) \\
&T_2 = \Big(0.54 \cdot 10^{-32} L2\, M^2 + 0.15 \cdot 10^{-41} L2^2 - 0.54 \cdot 10^{-32} L1\, L2^2 + 0.54 \cdot 10^{-32} L1\, M^2\Big) \\
&T_3 = 1555.39 \begin{pmatrix} 0.77 \cdot 10^{-21} L1\, L2 + 0.19 \cdot 10^{-39} - 0.39 \cdot 10^{-21} M^2 - 0.19 \cdot 10^{-21} L2 ... \\ -0.22 \cdot 10^{-30} L2 - 0.69 \cdot 10^{-30} L1 + 0.19 \cdot 10^{-21} L1^2 \end{pmatrix} \\
&T_4 = 39.44 \cdot \Big(0.33 \cdot 10^{-19} - 0.28 \cdot 10^{-10} L1 - 0.28 \cdot 10^{-10} L2\Big)
\end{aligned}
\tag{18}
$$

The generation of functional $f =$ *myfunL1L2M_PRL (x, fj)* serves the purpose of optimizing the APL $P_2 = P_{RL}$, which is a function of parameters L_1, L_2, and M. The implementation in MATLAB of the program called "main_gradient_L1L2M_PRL" must determine the values for parameters L_1, L_2, and M, corresponding to the optimal power transfer.

The program operates via routine *fminunc*, and the extracted values of L_1, L_2, and M are the optimum values. The parameters under scrutiny, subjected to the optimizing procedure, start from the following intervals of variations:

$$
\begin{aligned}
&L_1 \in [1.6e-05,\ 2.0e-05],\ L_2 \in [1.6e-05,\ 2.0e-05], \\
&M \in [1.4e-06,\ 1.8e-06]
\end{aligned}
$$

Table 5 contains the results following the running of the program mentioned above for the objective function from (15a), with a *frequency between 107 and 1.4*

Table 5 Parameters for active power optimization

Parameters for optimizing active power PRL	Parameters for optimizing active power PRL	Parameters for optimizing active power PRL
it_max = 41;	it_max = 42;	it_max = 13;
L1_max = 2.0 e-05 H	L1_max = 2.0 e-05 H	L1_max = 2.0 e-05 H
L 1n = 1.6748 e-05 H	L 1n = 1.6748 e-05 H	L 1n = 1.6748 e-05 H
L2_max = 2.0 e-05 H	L2_max = 2.0 e-05 H	L2_max = 1.8 e-05 H
L 2n = 1.6735 e-05 H	L 2n = 1.6735 e-05 H	L 2n = 1.6735 e-05 H
M_max = 1.4 e-06 H	M_max = 1.4 e-06 H	M_max = 1.4 e-06 H
Mn = 1.4899 e-06 H	Mn = 1.4899 e-06 H	Mn = 1.4899 e-06 H
k_max = 0.07	k_max = 0.07	k_max = 0.07
kn = 0.089	kn = 0.089	kn = 0.089
Parameters for optimizing active power PRL	Parameters for optimizing active power PRL	Parameters for optimizing active power PRL
it_min = 9	it_min = 16	it_min = 41
L1_min = 1.8 e-05 H	L1_min = 2.0 e-05 H	L1_min = 2.0 e-05 H
L 1n = 1.6748 e-05 H	L 1n = 1.6748 e-05 H	L 1n = 1.6748 e-05 H
L2_min = 2.0 e-05 H	L2_min = 2.0 e-05 H	L2_min = 2.0 e-05 H
L 2n = 1.6735 e-05 H	L 2n = 1.6735 e-05 H	L 2n = 1.6735 e-05 H
M_min = 2.0 e-06 H	M_min = 2.0 e-06 H	M_min = 2.0 e-06 H
Mn = 1.4899 e-06 H	Mn = 1.4899 e-06 H	Mn = 1.48990 e-06 H
k_min = 0.1	k_min = 0.1	k_min = 0.1
kn = 0.089	kn = 0.089	kn = 0.089

$\times$ *107* Hz*, and a frequency step of 0.2* $\times$ *107* Hz. To obtain the results, one applied three procedures used to calculate the Hessian matrix, included in the *fminunc* routine.

Figure 8 contains the variation of the with the frequency of APL P_{Lss}, respectively, of the efficiency *eta21ss* for the application of the third procedure of using the Hessian matrix 'HessUpdate','steepdesc' to the objective function (15a) for the frequency domain previously mentioned.

Consulting Table 5, one can remark the maximum values obtained for the active power P_{Lss} when the parameters L_1, L_2 and M have optimal values, being higher than the maximum of P_{Lss} corresponding to the nominal values of these parameters. The application of the same procedure for the objective functions (15b), (c), respectively (15d) delivered equivalent results summarized in Figs. 9, 10 and 11. When is analyzing Figs. 8, 9, 10, 11, one can find similar results for all four cases involving different objective functions.

Moreover, the results corresponding to the optimal values of parameters L_1, L_2, and M are practically identical for the three procedures for using the Hessian matrix (Table 5).

Whereas performing a thorough analysis of the results from Figs. 8, 9, 10, 11, one can extract interesting remarks:

1. The phenomenon of "splitting frequency" becomes evident for both sets of values of the parameters L_1, L_2, and M. The first set of values represents the nominal ones, whereas the second set of those corresponds to the maximum value of the power. Among the frequencies corresponding to the two maximum efficiency values recorded in this case is a significant difference.

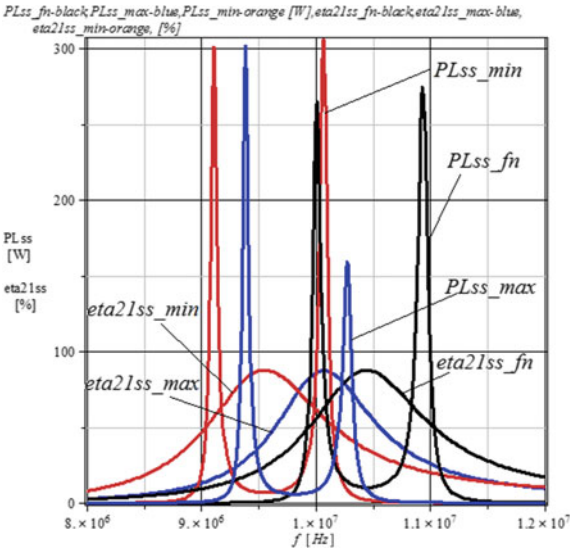

Fig. 8 Variations of APL and efficiency with the frequency for the objective function (19, a)-*optimum power*

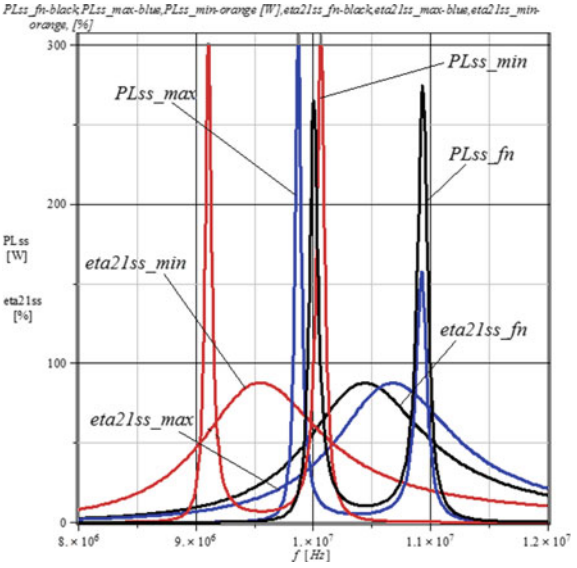

Fig. 9 Variations of APL and efficiency with frequency for the objective function (19, b)-*optimum power*

2. In the case when the parameters L_1, L_2, and M have the optimum values, the WPT efficiency has three maxima.
3. The second maximum value recorded for the APL is higher than the one corresponding to its first maximum.

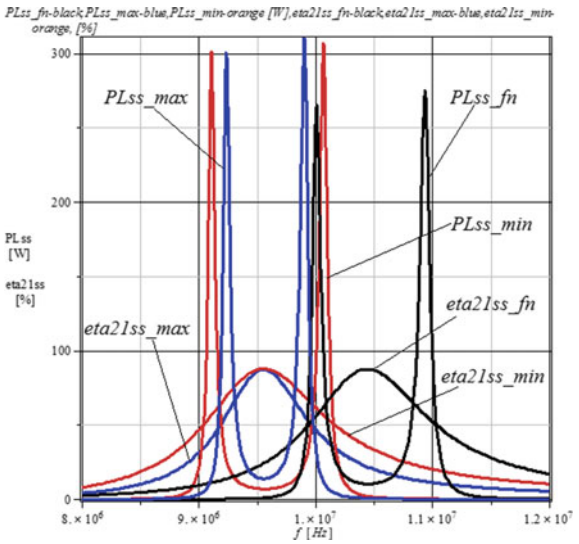

Fig. 10 Variations of APL and efficiency with the frequency for the objective function (19, c)-*optimum power*

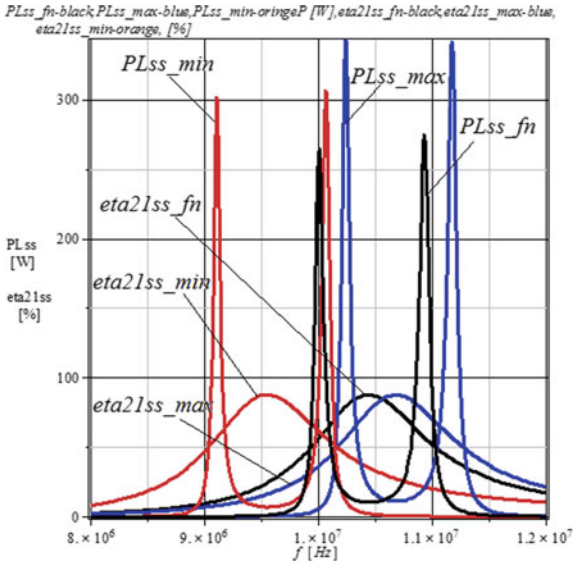

Fig. 11 Variations of APL and efficiency, with the frequency for the objective function (19, d)-*optimum power*

4. Looking at the values of the APL at the frequencies where the efficiency is maximum, one can observe a lower active power in for the optimal set of parameters L_1, L_2, and M, when compared to the case when the same parameters have nominal values.

5.2 *Efficiency Optimization Function of L1, L2, and M Parameters*

The WPT efficiency as a function of frequency, with unknown parameters L_1, L_2, and M is:

$$\begin{aligned} eta21ss\_L1L2M &:= 0.15 \cdot 10^{-15} f^4 M^2 / \left(T_5 f^4 + T_6 f^2 + 6.35\right) \\ T_5 &= 1555.39\left(0.12 \cdot 10^{-20} M^2 + 0.12 \cdot 10^{-20} L2^2\right) \\ T_6 &= 39.4384\left(-0.18 \cdot 10^{-9} L2 + 0.49 \cdot 10^{-19}\right) \end{aligned} \tag{19}$$

The generation of functional $f =$ *myfunL1L2M_eta21 (x, fj)* serves the purpose of optimizing the WPT efficiency, function of L_1, L_2, and M parameters. The implementation of the program called "main_gradient_L1L2M_eta21", must determine the values for parameters L_1, L_2, and M, corresponding to the optimal efficiency. The program, developed in MATLAB as well, operates via routine *fminunc* and the extracted values of L_1, L_2, and M are the optimum values.

The parameters under scrutiny, subjected to the optimizing procedure, start from the following intervals of variations:

$$\begin{aligned} &L_1 \in [1.6e-05,\ 1.8e-05],\ L_2 \in [1.6e-05,\ 1.8e-05], \\ &M \in [1.0e-06,\ 1.6e-06] \end{aligned}$$

Table 6 contains the results following the running of the program mentioned above for the objective function from (15a), with a *frequency between 107* Hz *and 1.4* $\times$ *107* Hz*, and a frequency step of 0.2* $\times$ *107* Hz. To obtain the results, one applied three procedures used to calculate the Hessian matrix, included in the *fminunc* routine.

Figure 12 contains the frequency variation of the active power *PLss*, respectively of the efficiency *eta21ss*, for the application of the third procedure of using the Hessian matrix 'HessUpdate','steepdesc' to the objective function (15a) for the frequency domain previously mentioned.

Consulting Table 6, one can remark the maximum values obtained for the efficiency *eta21ss* when the parameters L_1, L_2, and M have optimal values, being higher than the maximum of *eta21ss* corresponding to the nominal values of these parameters.

The application of the same procedure for the objective functions (15b), (15c), respectively (15d) delivered equivalent results summarized in Figs. 13, 14, and 15, respectively.

Analyzing Figs. 12, 13, 14, 15, one can find similar results for all four objective functions.

Moreover, the results corresponding to the optimal values of parameters L_1, L_2 and M are practically identical for the three procedures for using the Hessian matrix (Table 6).

Table 6 Parameters for efficiency optimizing

Parameters for optimizing the efficiency of eta21ss	Parameters for optimizing the efficiency of eta21ss	Parameters for optimizing the efficiency of eta21ss
it_max = 41;	it_max = 46;	it_max = 47;
L1_max = 1.6 e-05 H	L1_max = 1.8 e-05 H	L1_max = 2.0 e-05 H
L 1n = 1.6748 e-05 H	L 1n = 1.6748 e-05 H	L 1n = 1.6748 e-05 H
L2_max = 1.729 e-05 H	L2_max = 1.729 e-05 H	L2_max = 1.729 e-05 H
L 2n = 1.6735 e-05 H	L 2n = 1.6735 e-05 H	L 2n = 1.6735 e-05 H
M_max = 1.423 e-06 H	M_max = 1.423e-06 H	M_max = 1.423 e-06 H
Mn = 1.4899 e-06 H	Mn = 1.4899 e-06 H	Mn = 1.4899 e-06 H
k_max = 0.0855	k_max = 0.0806	k_max = 0.0806
kn = 0.089	kn = 0.089	kn = 0.089
Parameters for optimizing active power PRL	Parameters for optimizing active power PRL	Parameters for optimizing active power PRL
it_min = 49	it_min = 49	it_min = 46
L1_min = 1.6 e-05 H	L1_min = 1.6 e-05 H	L1_min = 1.8 e-05 H
L 1n = 1.6748 e-05 H	L 1n = 1.6748 e-05 H	L 1n = 1.6748 e-05 H
L2_min = 1.729 e-05 H	L2_min = 1.7294 e-05 H	L2_min = 1.729 e-05 H
L 2n = 1.6735 e-05 H	L 2n = 1.6735 e-05 H	L 2n = 1.6735 e-05 H
M_min = 1.423 e-06 H	M_min = 1.423 e-06 H	M_min = 1.423 e-06 H
Mn = 1.4899 e-06 H	Mn = 1.4899 e-06 H	Mn = 1.4899 e-06 H
k_min = 0.0855	k_min = 0.0855	k_min = 0.0807
kn = 0.089	kn = 0.089	kn = 0.089

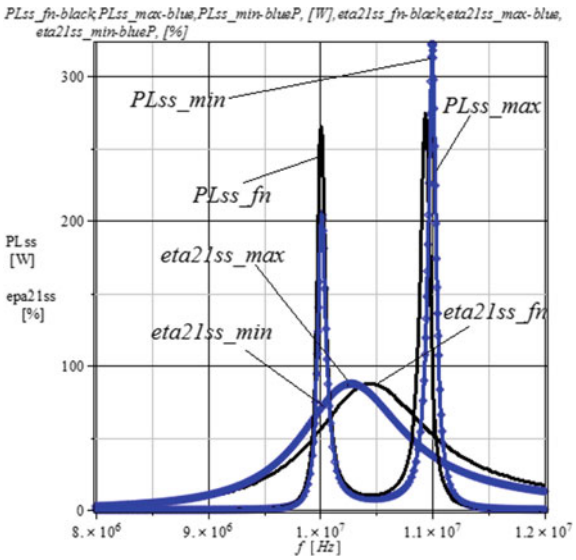

Fig. 12 The variations of the APL and efficiency with the frequency for the objective function (19, a)-*optimum efficiency*

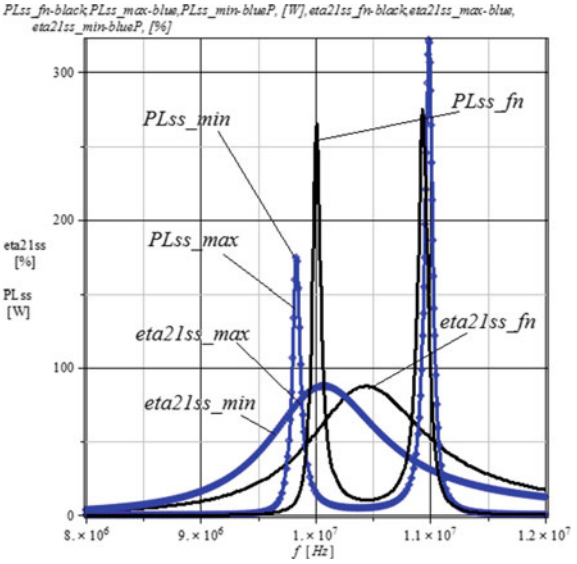

Fig. 13 The variations of the APL and efficiency with the frequency for the objective function (19, b)-*optimum efficiency*

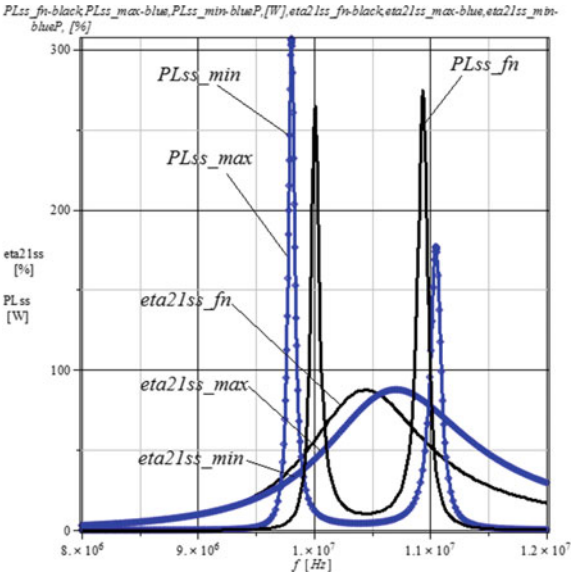

Fig. 14 The variations of the transmitted active power and efficiency with the frequency for the objective function (19, c)-*optimum efficiency*

Performing a thorough analysis of the results from Figs. 12, 13, 14, 15, one can extract interesting remarks:

1. The phenomenon of "splitting frequency" becomes evident for both sets of values of the parameters L_1, L_2, and M. The first set of values represents the nominal

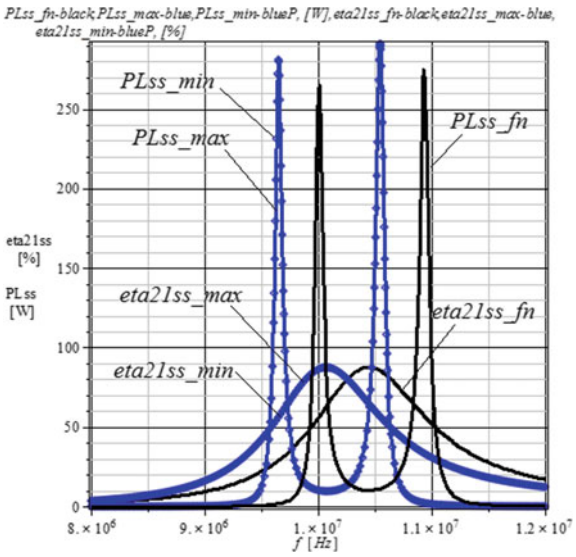

Fig. 15 The variations of the transmitted active power and efficiency with the frequency for the objective function (19, d)-*optimum efficiency*

ones, whereas the second set of those corresponds to the maximum value of the WPT efficiency.

2. In the case when the parameters L_1, L_2 and M have the optimum values, the WPT efficiency has three maxima.
3. The second maximum value recorded for the WPT efficiency is identical to the maximum WPT efficiency corresponding to the nominal values of the parameters.
4. The maximum values of the active power are lower for the optimal values of the parameters providing maximum efficiency than those corresponding to the nominal parameters.
5. The frequencies corresponding to the two maxima of the active power, for optimal parameters case, are different from those corresponding to the nominal parameters one.

5.3 Structure's Optimization Using ANSYS Q3D Extractor

When using ANSYS Q3D Extractor software, the mesh is essential for the accuracy of the solution. A major drawback of the program is given by the fact that the initial network can face convergence problems of an increased computational effort. The advantage of the mesh in ANSYS Q3D Extractor program is that the discretization of the coil takes place in the area of interest. So, it is no need to discretize the air in the vicinity of the coil or use conditions indefinitely. The resulting RLC matrices let us generate new matrices for any named parameters with field solutions, without having to compute new field solutions. Besides, any model successfully solved can have its matrix results exported to an equivalent circuit for further signal integrity

analysis. After the field solutions and matrix calculations are complete, the simulator performs an error analysis in each element in the mesh. Upon the next adaptive pass, there is a refinement process targeting the elements with the highest error. Therefore, in those areas, the obtained solution is more accurate.

The study from this section denotes the utilization of the program ANSYS Q3D EXTRACTOR [30–33] to simulate the WPT between differently configured two coils at three frequencies: *50* kHz, *5000* kHz, and *10,000* kHz. The best four configurations (cases) selected from a preliminary analysis are:

1. *Two spiral parallel coils*
2. *Two truncated cone-like coils with parallel bases, configuration A*
3. *Two truncated cone-like coils with non-parallel bases*
4. *Two truncated cone-like coils with parallel bases, configuration B*

1. *Two spiral parallel coils.* The constructive characteristics of the configuration: turn's initial radius $r = 10$ mm, pitch $p = 0.21$ mm, wire Sect. 0.2×0.2 mm^2, distance between coils $z = 20$ mm, and number of turns $N = 15$ (see Fig. 16). The determination of parameters for the configuration displayed in Fig. 16, using ANSYS Q3D EXTRACTOR [30–33] resulted in the values filling Table 7.
2. *Two truncated cone coils-like coils with the parallel bases, configuration A.* The constructive characteristics: turn's initial radius of a turn $r = 10$ *mm*, the distance between the centres of the two consecutive turns *0.21* mm, the distance between the centres of the two consecutive turns on the 0Y axis *0.21 mm*, the wire Sect. 0.2×0.2 mm^2, the distance between the coils $z = 20$ mm, and the number of turns $N = 15$. (see Fig. 17).

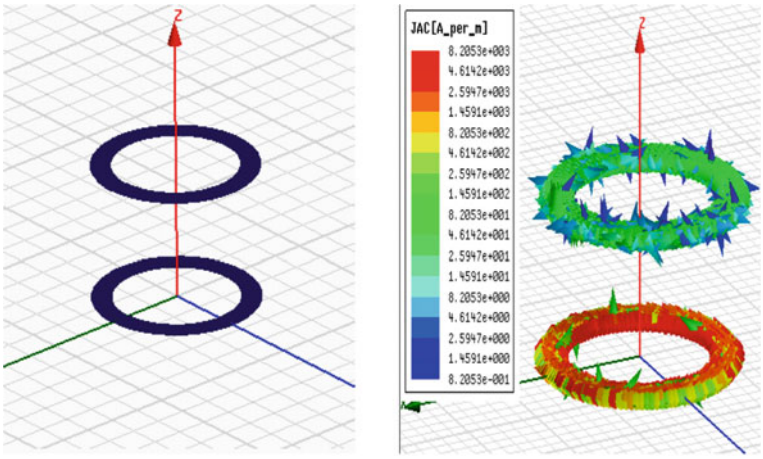

Fig. 16 **a** Configuration of the 2 spiral parallel coils; **b** Current density surface

Table 7 Results for spiral parallel coils

Frequency f [kHz]	50	5000	10,000
Resistance matrix [ohm]	$\begin{pmatrix} 0.1635 & 0.0004 \\ 0.0009 & 0.1790 \end{pmatrix}$	$\begin{pmatrix} 2.1451 & 0.0394 \\ 0.0394 & 2.3414 \end{pmatrix}$	$\begin{pmatrix} 7.7438 & 0.1892 \\ 0.1892 & 7.6332 \end{pmatrix}$
Capacity matrix [pF]	$\begin{pmatrix} 0.9601 & -0.2977 \\ -0.2977 & 0.9602 \end{pmatrix}$	$\begin{pmatrix} 0.9601 & -0.2977 \\ -0.2977 & 0.9602 \end{pmatrix}$	$\begin{pmatrix} 0.9601 & -0.2977 \\ -0.2977 & 0.9602 \end{pmatrix}$
Inductivity matrix [μH]	$\begin{pmatrix} 8.8699 & 0.4971 \\ 0.4971 & 8.8821 \end{pmatrix}$	$\begin{pmatrix} 8.5028 & 0.4950 \\ -0.75045 & 8.5032 \end{pmatrix}$	$\begin{pmatrix} 8.7034 & 0.4927 \\ 0.4927 & 8.7154 \end{pmatrix}$

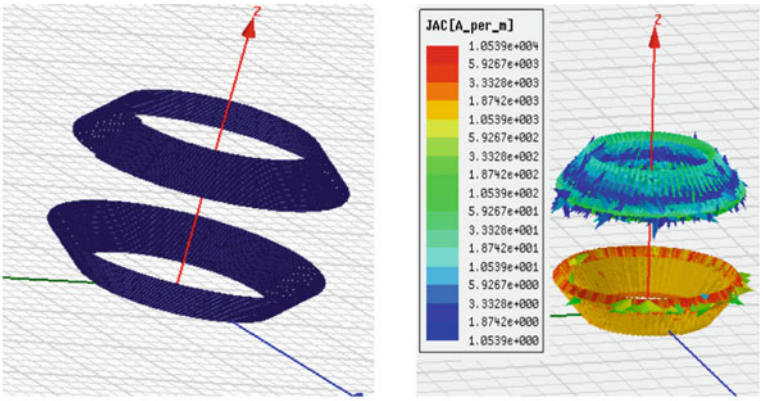

Fig. 17 **a** Truncated cone-like coils with the parallel bases, configuration 1; Current density surface

The determination of the parameters for the configuration displayed in Fig. 17, using ANSYS Q3D EXTRACTOR [30–33] resulted in the values filling Table 8.

3. *Two truncated cone-like coils with the nonparallel bases*, one of them is rotated with an angle of 45^0. The constructive characteristic of the configuration are: the initial radius of a turn $r = 10$ mm, the distance between the centres of the two consecutive turns 0.21 mm, the distance between the centres of the two consecutive turns on the 0Y axis 0.21 mm, the wire Sect. $0.2 \times 0\ 0.2\ mm^2$, the distance between the coils $z = 20\ mm$, and the turn number N = 15 (see Fig. 18). The determination of parameter for the configuration displayed in Fig. 18, using ANSYS Q3D EXTRACTOR [30–33] resulted in the values filling the Table 9.
4. *Two truncated cone-like coils with the parallel bases, configuration 2*. The constructive characteristics of the configuration are: the distance on the 0Z: $z = 20$ mm and the distance on the 0Y is $y = 15$ mm, the coil's initial radius of

Table 8 Results obtained for configuration A

Frequency f [kHz]	50	5000	10,000
Resistance matrix [ohm]	$\begin{pmatrix} 0.1826 & 0.0012 \\ 0.0012 & 0.1807 \end{pmatrix}$	$\begin{pmatrix} 2.4503 & 0.0772 \\ 0.0772 & 2.5167 \end{pmatrix}$	$\begin{pmatrix} 4.1709 & 0.1374 \\ 0.1374 & 4.0615 \end{pmatrix}$
Capacity matrix [pF]	$\begin{pmatrix} 1.3023 & -0.5986 \\ -0.5986 & 1.3031 \end{pmatrix}$	$\begin{pmatrix} 1.3023 & -0.5986 \\ -0.5986 & 1.3031 \end{pmatrix}$	$\begin{pmatrix} 0.9601 & -0.2977 \\ -0.2977 & 0.9602 \end{pmatrix}$
Inductivity matrix [μH]	$\begin{pmatrix} 13.348 & -1.9729 \\ -1.9729 & 13.339 \end{pmatrix}$	$\begin{pmatrix} 13.0880 & -1.9689 \\ -0.5986 & 13.173 \end{pmatrix}$	$\begin{pmatrix} 13.4930 & -1.9727 \\ -1.9727 & 13.5310 \end{pmatrix}$

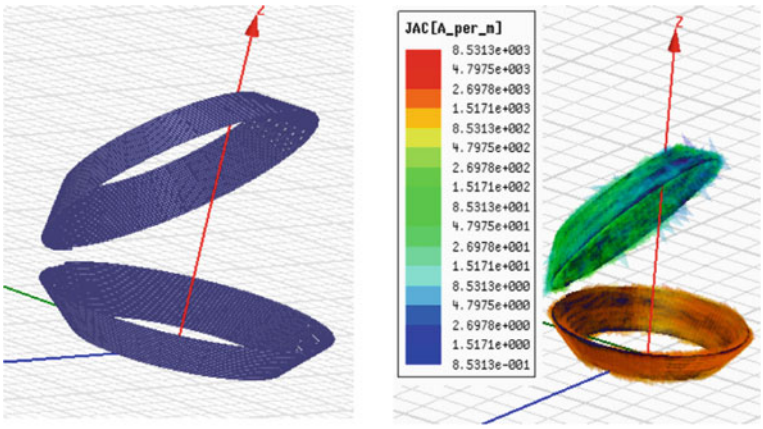

Fig. 18 **a** Truncated cone-like coils with nonparallel bases, one of them are rotated with an angle of 45^0; **b** Current density surface

Table 9 The results obtained for the truncated cone-like coils, with the nonparallel bases, one of them is rotated with an angle of 45°

Frequency f [kHz]	50	5000	10,000
Resistance matrix [ohm]	$\begin{pmatrix} 0.1846 & 0.0015 \\ 0.0015 & 0.1787 \end{pmatrix}$	$\begin{pmatrix} 2.3284 & 0.0196 \\ 0.0196 & 2.3955 \end{pmatrix}$	$\begin{pmatrix} 4.5941 & 0.2569 \\ 0.2569 & 4.9967 \end{pmatrix}$
Capacity matrix [pF]	$\begin{pmatrix} 1.3743 & -0.6593 \\ -0.6593 & 1.3667 \end{pmatrix}$	$\begin{pmatrix} 1.3743 & -0.6593 \\ -0.6593 & 1.3667 \end{pmatrix}$	$\begin{pmatrix} 1.3743 & -0.6593 \\ -0.6593 & 1.3667 \end{pmatrix}$
Inductivity matrix [μH]	$\begin{pmatrix} 13.3680 & 1.8555 \\ 1.8555 & 13.3730 \end{pmatrix}$	$\begin{pmatrix} 13.2090 & -1.9689 \\ 1.8560 & 13.0710 \end{pmatrix}$	$\begin{pmatrix} 13.5420 & 1.8485 \\ 1.8485 & 13.4200 \end{pmatrix}$

the turn is $r = 10$ mm, the distance between the centres of the two consecutive turns 0.21 mm, the section of the wire 0.2×0.2 mm^2 and the number of turns $N = 15$ (see Fig. 19).

The determination of the parameters for the configuration displayed in Fig. 19, using ANSYS Q3D EXTRACTOR [30–33] resulted in the values filling Table 10.

Due to the highest value of the mutual inductance, $M = 1.9729$ μH (Table 9) between the two magnetic coupled coils (resonators), the second configuration (see Fig. 17) appears to be the best possible out of the four studied configurations of coils. Whereas assessing the parameter values determined through ANSYS Q3D EXTRACTOR simulations performed at the three mentioned frequencies, one can conclude that the values of the parameters (L, M, C) remain unchanged, yet the

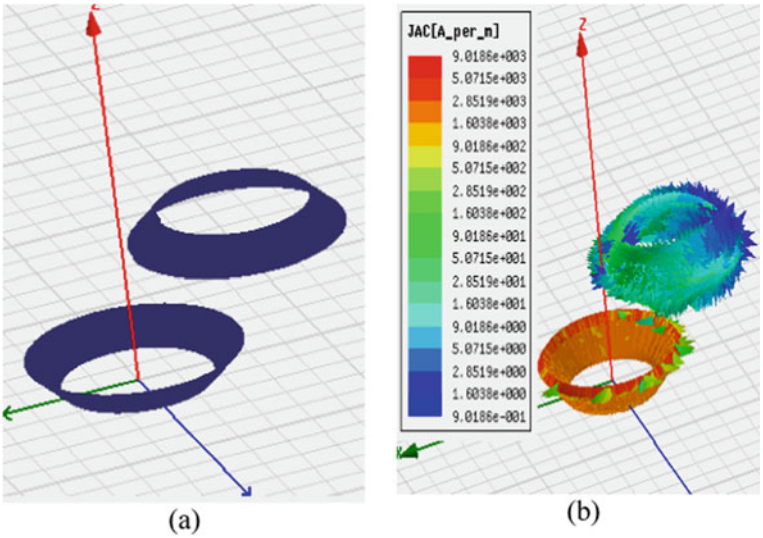

Fig. 19 **a** Truncated cone-like coils with the parallel bases, configuration B, **b** Surface current density

Table 10 Results obtained for configuration B

Frequency f [kHz]	50	5000	10,000
Resistance matrix [ohm]	$\begin{pmatrix} 183.3 & 0.9199 \\ 0.9199 & 181 \end{pmatrix}$	$\begin{pmatrix} 2720 & 32.731 \\ 32.731 & 2144.7 \end{pmatrix}$	$\begin{pmatrix} 4655.2 & 132.27 \\ 132.27 & 4715.4 \end{pmatrix}$
Capacity matrix [pF]	$\begin{pmatrix} 1.1973 & -0.4423 \\ -0.5523 & 1.975 \end{pmatrix}$	$\begin{pmatrix} 1.1973 & -0.4423 \\ -0.5523 & 1.975 \end{pmatrix}$	$\begin{pmatrix} 1.1973 & -0.4423 \\ -0.5523 & 1.975 \end{pmatrix}$
Inductivity matrix [μH]	$\begin{pmatrix} 13.366 & 0.6389 \\ 0.6389 & 13.347 \end{pmatrix}$	$\begin{pmatrix} 13.183 & 0.6387 \\ 0.6387 & 13.185 \end{pmatrix}$	$\begin{pmatrix} 13.4930 & 0.6357 \\ 0.6357 & 13.489 \end{pmatrix}$

Table 11 The mutual inductance: Values obtained through simulation versus measured

Method	1st Case	2nd Case	3rd Case	4th Case
M_m [μH]	0.5004	1.9875	1.8844	0.6482
M_p [μH]	0.4985	1.9862	1.876	0.6445
MQ3D [μH]	0.4971	1.9729	1.8555	0.6389

resistance sharply increases with the frequency due to the skin, respectively the proximity effect.

Table 11 contains the values of the mutual inductance (by measurements (M_m)), computed by integrating (M_p) in MATLAB, respectively and the ones obtained through simulations performed with ANSYS Q3D EXTRACTOR (*MQ3D*).

The values of mutual inductances determined with all three methods are very close for all four cases of coil configurations, suggesting compatibility of the three methods of determination.

6 Conclusions

The WPT's efficiency, function of frequency, is greatly influenced by the resonator parameters (L – self-inductance, M – mutual inductance, C – parasitic capacitance, and R – Ohmic resistances) of the coils, placed at different distances and angles in assemblies with several configurations. Consequently, parameter identification represents an essential objective during the configuration design stage.

The determination of the best possible configuration from a pool of four relied on the utilization of the ANSYS Extractor Q3D. The computation took place for the corresponding matrices for different configurations, structures, frequencies and distances between the resonators. Each configuration maintained the same relative position between the coils, the same number of turns, the same geometrical dimensions, and materials for conductors. The selected configuration, declared optimal, holds the highest mutual inductance between the coupled magnetic coils.

The optimization study had two directions. In the first direction of the study, one assessed the optimal parameter determination for the given configuration of two magnetically coupled coils, following two different outcomes: the maximum power transfer, respectively the maximum efficiency. The simulated tests involved the presence of four different objective functions for each of the outcomes and revealed interesting conclusions included together with the results. The second direction from the final part of the optimization study represented a simulation performed utilizing the ANSYS Q3D Extractor software. The output of the simulation consisted of sets of parameters as self-inductance, mutual inductance, capacitance, and resistance as a function of frequency. The coil resistance presents a strong dependency on the frequency due to the skin and proximity effects, whereas the other parameters maintain their constant values against frequency. Some factors are exercising a significant

influence on the mutual inductance parameter. They are the relative distance between the coils and the angle at which the field lines go through the receiver coil. The mutual inductance is a crucial parameter concerning the performances of WPT systems (i.e., the load power, the efficiency).

The mutual inductances computed with MATLAB utilizing the integration, the numerically calculated ones using ANSYS Q3D Extractor, and respectively those obtained through measurements show close values, indicating a consistency regarding all three methods of parameter determination.

References

1. Agbinya JI (2012) Wireless power transfer. River Publishers Series in Communications, 9000, Aalborg, Denmark
2. Kim KY (2011) Wireless power transfer—principles and engineering explorations. Published by InTech Janeza Trdine 9, 51000 Rijeka, Croatia
3. Zhang Z, Pang H, Georgiadis A, Cecati C (2019) Wireless power transfer—an overview. IEEE Trans Ind Electron 66(2):1044–1058
4. Zhang F, Liu L, Hackworth SA, Sclabassi RJ, Sun M (2009) In vitro and in vivo studies on wireless powering of medical sensors and implantable devices. In: Proceedings of life science systems and applications workshop. IEEE Xplore, 978-1-4244-4293-5/09/2009, pp 84−87
5. Karalis A, Joannopoulos JD, Soljačić M (2008) Efficient wireless non-radiative mid-range energy transfer. Ann Phys 323:34–48
6. Kurs A, Karalis A, Moffatt RA, Joannopoulos JD, Fisher P, Soljačić M (2007) Wireless power transfer via strongly coupled magnetic resonances. Science 317(5834):83–86
7. Moffatt RA (2009), Wireless transfer of electric power. Thesis for bachelor of science in physics (under the supervision of Soljačić M), MIT, Cambridge, MA, US
8. Tesla N (1914) Apparatus for transmitting electrical energy. US patent number1119732
9. https://www.witricity.com
10. https://electronicsca.blogspot.com/2015/07/wireless-power-transmission-market.html
11. Ochiana G, Ochiana L, Stănculescu M (2012) Electromagnetic field theory, Editura Printech, ISBN 978-606-521-879-6, 202
12. Jiang HC, Wang YC (2008) Capacity performance of an inductively coupled near field communication system. Proc IEEE Int Symp Antenna Propag Soc 1:1–4
13. Imura T, Hori Y (2011) Maximizing air gap and efficiency of magnetic resonant coupling for wireless power transfer using equivalent circuit and Neumann formula. IIEEE Trans Ind Electron 58(10):4746–4752
14. Cheon S, Kim YH, Kang SY, Lee ML, Lee JM, Zyung T (2011) Circuit model based analysis of a wireless energy transfer system via coupled magnetic resonances. IEEE Trans Ind Electron 58(7):2906–2914
15. Imura T, Okabe H, Hori Y (2009) Basic experimental study on helical antennas of wireless power transfer for electric vehicles by using magnetic resonant couplings. In: Proceedings of vehicle power and propulsion conference, pp 936–940. IEEE Xplore 978-1-4244-2601-4/010/2010
16. Mercier PP, Chandrakasan AP (2013) Rapid wireless capacitor charging using a multi-tapped inductively secondary coil. IEEE Trans Circuits Syst-I 60(9):2263–2272
17. Sample AP, Meyer DA, Smith JR (2011) Analysis, experimental results, and range adaptation of magnetically coupled resonators for wireless power transfer. IEEE Trans Ind Electron 58(2):544–554

18. Ricano JA, Rodriguez Torres H, Vazquez Leal H, Gallardo del Angel A (2010) Experiment about wireless energy transfer. In: 1st international congress on instrumentation and applied sciences, Cancun, Mexico, pp 1–10. Oct 26–29 2010
19. Bobaru L (2017) Magnetically coupled resonator coils optimization used in wireless power transfer systems, PhD Thesis, University Politehnica of Bucharest, Romania
20. Iordache M, Bucată V, Niculae D, Stănculescu M, Bobaru LM (2108) Design of wireless electromagnetic energy transfer systems, annals of the university of Craiova. Electr Eng Ser 42(1):15–20
21. Niculae D, Stănculescu M, Mihai Iordache M, Bobaru ML (2018) An analysis on efficiency of wireless transfer energy due to a misalignment of two coils annals of the university of Craiova. Electr Eng Ser 42(1):21–25
22. Stănculescu M, Bobaru L, Iordache M, Niculae D, Bucată V (2018) Wireless Power Transfer Analysis Using Scattering Parameters annals of the university of Craiova. Electr Eng Ser 42(1):26–31
23. Iordache M, Andronescu G, Bucata V, Iordache (Bobaru) ML, Stanculescu M, Niculae D, (2016) Design and simulation of wireless power transfer systems, annals of the university of Craiova. Electr Eng Ser 40(1):109–114
24. Bibirică C, Sandu C, Ene L, Iordache M (2017) Improving the performance of PCB inductors for WPT systems using magnetic shields. In: Proceedings of 5th international symposium on electrical and electronics engineering (ISEEE). Galați, Romania, pp 1–7. Oct 20–22 2017
25. Iordache (Bobaru) L, Iordache M (2016) Optimization of magnetic coupled resonator structure used in wireless electromagnetic energy transfer, U.P.B. Sci Bull Ser C – Electr Eng 78(4):137–148
26. Stanculescu M, Iordache M, Niculae D, Bobaru L, Bucata V (2018) Algorithm for computing s parameters and their use for studying efficiency of electromagnetic energy wireless transfer systems. Rev Roumaine Sci Tech. Serie Electrotechnique et Energetique, 63(2):138–144
27. Stanculescu M, Iordache M, Niculae D, Iordache Bobaru L, Bucata V (2016) Parameter computation and their use for electromagnetic energy wireless transmission. Int J of Comput Technol 15(9)
28. Iordache M (2015) Symbolic, numeric—symbolic and numeric simulation of analog circuits—user guides. MATRIX ROM, Bucharest, Romania
29. Niculae D, Iordache M, Dumitriu L (2011) Magnetic coupling analysis in wireless transfer energy, the 7th international symposium on advanced topics in electrical engineering (ATEE), May 12–14 2011. Bucharest, Romania, pp 1–4
30. Ansoft Q3D Extractor, *User Guide*, https://www.ansoft.com
31. ***Geting Started with Q3D Extractor A 3D PCB Via Model, ANSYS,* Inc. 275 Technology Drive, Canonsburg, PA 15317 USA, 2011
32. https://www.ansoft.com/ansoftdesignersv
33. https://www.ansys.com/Products/Simulation+Technology/Systems+&+Embedded+Software/ANSYS+Simplorer.
34. Iordache M, Dumitriu L (2014) Computer-aided simulation of analog circuits—algorithms and computational techniques, Editura POLITEHNICA Press, vol. I and II, Bucharest, Romania
35. Iordache M (2016) Special works of electrotehnics. MATRIX ROM, Bucharest, Romania
36. Iordache M, Dumitriu L, Delion D (2000) SESYMGP-state equation symbolic generation program. Politehnica University of Bucharest, Romania, User Guide. Library of Electrical Department
37. Iordache M, Dumitriu L, Matei I (2002) SYMNAP– symbolic modified nodal analysis program. Politehnica University of Bucharest, User Guide. Library of Electrical Department
38. ***Optimization Toolbox™ User's Guide*, Matlab R2011b, The Math Works, Inc., 2011
39. Orasanu A, Dragomir A, Bobaru L, Iordache M, Deleanu S (2018) On optimization of wireless power transfer systems, 2018 international symposium on fundamentals of electrical engineering (ISFEE), Nov 1–3 2018. Bucharest, Romania, pp 1–6
40. Iordache M, Dumitriu L, Niculae D (2016) Chapter 1 "Power transfer by magnetic induction using coupled-mode theory", Book chapter in the book, *Wireless Power Transfer*, 2nd edn, Editor J. I. Agbinya, River Publishers Series in Communications, Denmark, (1), pp 1–69

41. Iordache M, Niculae D, Ene L, Sandu C, Bobaru L, Bibirică C (2017) On the procedures for optimal wireless energy transfer systems. In: Proceedings of electric vehicle international conference and show. Bucharest. Romania, pp 1–6. Oct 5–6 2107